SageAttention2: Efficient Attention with Thorough Outlier Smoothing and Per-thread INT4 Quantization

Jintao Zhang*, Haofeng Huang*, Pengle Zhang, Jia Wei, Jun Zhu, Jianfei Chen Tsinghua University

Abstract

Although quantization for linear layers has been widely used, its application to accelerate the attention process remains limited. To further enhance the efficiency of attention computation compared to SageAttention while maintaining precision, we propose SageAttention2, which utilizes significantly faster 4-bit matrix multiplication (Matmul) alongside additional precision-enhancing techniques. First, we propose to quantize matrixes (Q,K) to INT4 in a hardware-friendly thread-level granularity and quantize matrixes (\tilde{P},V) to FP8. Second, we propose a method to smooth Q, enhancing the accuracy of INT4 QK. Third, we propose to use an FP32 Matmul buffer for PV to enhance the accuracy of FP8 $\tilde{P}V$. The operations per second (OPS) of SageAttention2 surpass FlashAttention2 and xformers by about $\mathbf{3x}$ and $\mathbf{5x}$ on RTX4090, respectively. Comprehensive experiments confirm that our approach incurs negligible end-to-end metrics loss across diverse models—including those for large language processing, image generation, and video generation. The codes are available at https://github.com/thu-ml/SageAttention.

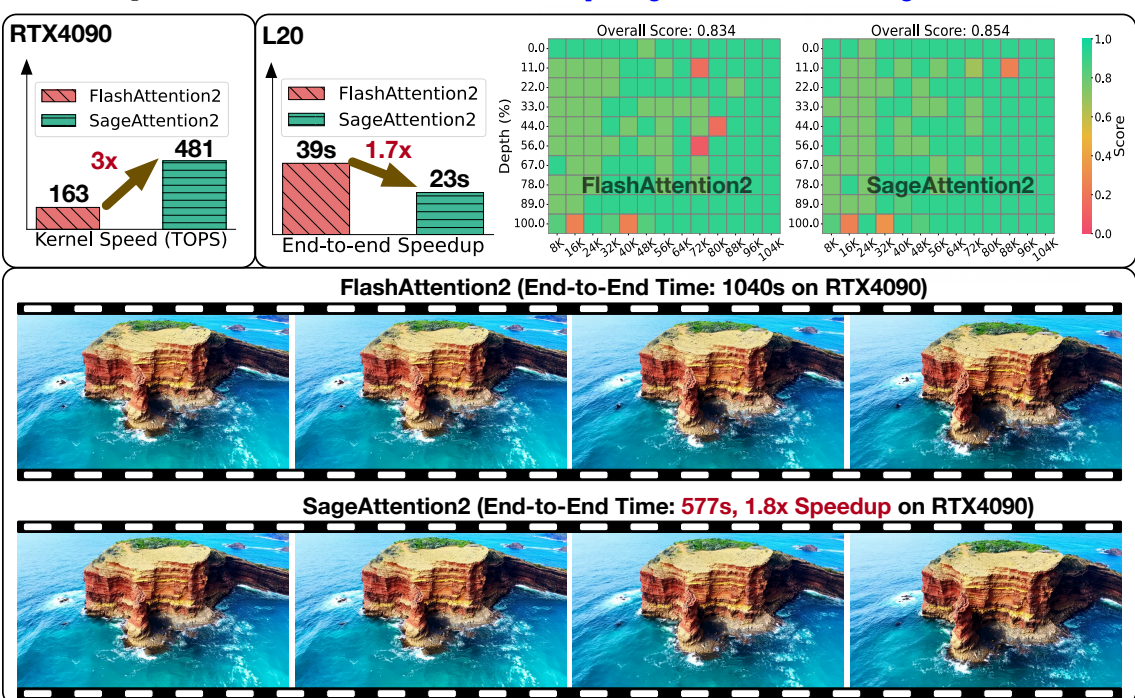


Figure 1: The upper left figure shows the kernel speedup on RTX4090 GPU. The upper right figure shows the end-to-end inference speedup of generating the first token and performance metrics for the needle-in-a-haystack task (gkamradt, 2023) with a sequence length of 100K on Llama3.1 on L20 GPU. The figure below shows two videos generated by CogvideoX (1.5-5B) using FlashAttention2 and SageAttention2 on RTX4090, showing that SageAttention2 accelerates generation 1.8x with no video quality loss.

^{*} Equal Contribution.

1 Introduction

Due to the quadratic time complexity of attention, efficiently implementing it becomes crucial as sequence lengths increase in real-world applications (Jiang et al., 2024). Several strategies have been developed to mitigate computational demands of attention —such as (1) Linear attention methods (Wang et al., 2020; Choromanski et al., 2020; Yu et al., 2022; Katharopoulos et al., 2020) that reduce complexity to O(N) and (2) Sparse attention methods (Liu et al., 2021; Chu et al., 2021; Li et al.; Xiao et al., 2023b, 2024; Chen et al., 2023; Jiang et al., 2024; Venkataramanan et al., 2023; Gao et al., 2024; Fu et al., 2024) that selectively process parts of the context — these methods are only suitable for a limited range of models and tasks. Widely used attention methods optimize attention by exploiting hardware capacities to enhance the computation speed, such as FlashAttention (Dao et al., 2022), FlashAttention2 (Dao, 2023), FlashAttention3 (Shah et al., 2024), xformers (Lefaudeux et al., 2022), and SageAttention (Zhang et al., 2024). Those works do not omit the computation of attention over parts of the context and achieve impressive speed and precision performance across various models and tasks.

Motivation. For the two matrix multiplication (Matmul) operations in attention: QK^{\top} and $\tilde{P}V$, SageAttention accelerates them by quantizing the QK^{\top} to INT8 and uses FP16 Matmul with FP16 accumulators for $\tilde{P}V$. Moreover, to keep the accuracy of attention, SageAttention proposes smoothing K by eliminating its channel-wise outliers. SageAttention achieves $2 \times$ and $2.7 \times$ speedup than FlashAttention2 and xformers and is the first quantized attention that incurs negligible end-to-end metrics loss across language, image, and video generation models. However, SageAttention has two weaknesses. (W1) INT8 Matmul achieves only half the speed of INT4. (W2) FP16 Matmul with FP16 accumulators is only compatible with RTX4090 and RTX3090 GPUs. To leverage the faster INT4 tensor cores for QK^{\top} and using a method that can accelerate $\tilde{P}V$ on a broader range of GPUs, we propose SageAttention2, which quantizes Q, K to INT4 and \tilde{P}, V to FP8

Challenges. Quantizing Q, K to INT4 and \widetilde{P}, V to FP8 presents significant challenges. For example, when only per-tensor quantizing Q, K to INT4, the text-to-video model CogvideoX will generate a completely blurry video (See Figure 2), and Llama2 only achieves a random-guessing-level accuracy of 25% on MMLU. After investigating deeply, we identified three primary challenges: (C1) The numerical range of INT4 is quite limited compared to FP16 or INT8, leading to significant quantization errors when Q and K have some abnormal values. (C2) We discover that the FP32 accumulator designed for FP8 matrix multiplication in the tensor core (mma.f32.f8.f32) is actually FP22, specifically with 1 sign bit, 8 exponent bits, and 13 mantissa bits. This will lead to an accuracy loss of $\widetilde{P}V$.

Quantizing Q,K to INT4 directly Use SageAttention2

Figure 2: An example of quantizing Q, K to INT4 from CogvideoX.

<u>Our approach</u>. To address (C1), we first discovered that the per-block quantization of Q, K in SageAttention does not achieve sufficient accuracy for INT4 quantization. Simultaneously, to avoid the extra latency caused by per-token dequantization, where each GPU thread corresponds to multiple quantization scales, we propose an adequately precise quantization method that incurs no additional dequantization overhead. Specifically, we introduce a per-thread quantization approach based on the mapping between the GPU thread and memory layout of matrices as dictated by the PTX mma instructions. This method groups tokens cor-

responding to the same thread for quantization and dequantization, ensuring that each thread is associated with a single quantization scale. This approach achieves much better accuracy performance than per-block quantization with no additional dequantization overhead. Second, for the significant channel-wise outliers in matrices Q and K, we adopt smoothing K in SageAttention and propose an effective method to remove these outliers in Q. Specifically, we propose subtracting the average value of the channel dimension of Q, referred to as \overrightarrow{Q}_m . Then, we add $\overrightarrow{Q}_m K$ after the QK Matmul to ensure the correctness of the attention computation. To address (C2)—the accuracy loss from using a 22-bit accumulator for FP8 Matmul of PV—, we propose to use an FP32 buffer to accumulate the values from the 22-bit accumulator after each block Matmul of $\tilde{P}V$. This method confines the errors to the block range. Additionally, we design an optional technique to enhance the accuracy of the 22-bit accumulator. Specifically, we could smooth V by subtracting the average value of its channel dimension and adding the subtracted item to the attention output to maintain the correctness. Performance. Importantly, we offer a high-performance implementation of SageAttention2 on RTX4090 and L20 GPUs. This implementation achieves a peak performance of 481 TOPS on the RTX4090, outperforming FlashAttention2 and xformers by approximately 3x and 5x, respectively. Note that FlashAttention3 is tailored to and can only be used with the Nvidia Hopper architecture, i.e., H100 and H800. We extensively evaluate the end-to-end metrics of state-of-the-art text, image, and video generation models using SageAttention2. Across all models and tasks, SageAttention2 can be directly adopted in a plug-and-play manner with negligible loss in model performance.

2 Preliminary

2.1 FlashAttention

The computation of self-attention can be formulated as follows: $S = QK^{\top}/\sqrt{d}$, $P = \sigma(S)$, O = PV, where $\sigma(S)_{ij} = \exp(S_{ij})/\sum_k \exp(S_{ik})$ is the softmax operation. The matrices Q, K, and V each have dimensions $N \times d$, while the matrix S, P are $N \times N$. While d is typically small, e.g., 64 or 128, N can be millions. Therefore, the $N \times N$ matrices (S, P) are much larger than (Q, K, V), and a naive implementation suffers from the huge amount of global memory IO for (S, P) reads/writes. FlashAttention (Dao, 2023) proposes to tile Q, K, and V from the token dimension into blocks $\{Q_i\}, \{K_i\}, \{V_i\}$ with block size of b_q , b_k , b_v , respectively, where $b_k = b_v$. Then, to avoid the memory IO for (S, P), it uses online softmax (Milakov & Gimelshein, 2018) to progressively compute each block of O, i.e., O_i :

First, for each block of $\{K_i\}$, $\{V_i\}$, it computes the following equations iteratively:

$$\begin{split} S_{i}^{j} &= Q_{i} K_{j}^{\top} / \sqrt{d}, \quad (m_{i}^{j}, \widetilde{P}_{i}^{j}) = \widetilde{\sigma}(m_{i}^{j-1}, S_{i}^{j}), \quad l_{i}^{j} = \exp(m_{i}^{j-1} - m_{i}^{j}) l_{i}^{j-1} + \operatorname{rowsum}(\widetilde{P}_{i}^{j}), \\ O_{i}^{j} &= \operatorname{diag}\left(\exp(m_{i}^{j-1} - m_{i}^{j})\right) O_{i}^{j-1} + \widetilde{P}_{i}^{j} V_{j} \end{split}$$

Where m_i^j and l_i^j are $b_q \times 1$ vectors, which are initialized to $-\infty$ and 0 respectively. The $\tilde{\sigma}()$ is an online softmax operator: $m_i^j = \max\{m_i^{j-1}, \operatorname{rowmax}(S_i^j)\}, \ \tilde{P}_j^i = \exp(S_i^j - m_i^j).$

Finally, the output O_i can be computed by $O_i = \operatorname{diag}(l_i^j)^{-1}O_i^j$.

2.2 Quantization

A matrix multiplication C = AB can be accelerated with quantization as:

$$(\delta_A, \hat{A}) = \psi(A), \quad (\delta_B, \hat{B}) = \psi(B), \quad \hat{C} = \hat{A}\hat{B}, \quad C = \psi_{\delta_A \delta_B}^{-1}(\hat{C})$$
 (1)

 ψ is a quantizer which converts a high-precision (e.g., FP32 or FP16) matrix A to a low-precision format \hat{A} (e.g., INT4 or FP8) with a scale δ_A , and ψ^{-1} is a dequantizer to convert back to high-precision. We should have $\psi_{\delta_A}^{-1}(\hat{A}) \approx A$. The actual matrix multiplication $\hat{A}\hat{B}$ is carried in low precision. In modern GPUs, low-precision matrix multiplication is usually multiple times faster than higher-precision ones. Many quantizers

depend on the numerical format and granularity, e.g., how many elements share a common scale factor. For example, an INT4 per-tensor quantizer first computes the scale as the maximum absolute value of the entire tensor, scales the elements to the maximum representable range of INT4 [-7, +7], and then casts to INT4 with rounding: $\hat{A} = \lceil A/\delta_A \rfloor$, $\delta_A = \max(|A|)/7$. Likewise, per-token quantizer assigns a scale factor for each token of a tensor: $\hat{A}[i,:] = \lceil A[i,:]/\delta_A[i] \rfloor$, $\delta_A[i] = \max(|A[i,:]|)/7$. Also, per-channel quantizer assigns a scale factor for each channel of the tensor, i.e., along the channel dimension: $A[:,i] = \lceil A[:,i]/\delta_A[i] \rfloor$, $\delta_A[i] = \max(|A[:,i]|)/7$. The dequantization process is an element-wise scaling. For example, for per-tensor dequantization, $\psi_{\delta_A\delta_B}^{-1}(\hat{A}\hat{B}) = \hat{A}\hat{B} * \delta_A * \delta_B$.

2.3 SageAttention

Based on the block tiling in FlashAttention2 (Dao, 2023), SageAttention (Zhang et al., 2024) quantize Q, K to INT8 in a per-block granularity. Moreover, to keep the quantization accuracy, SageAttention proposes to smooth K first:

$$K = K - \operatorname{mean}(K)$$

$$\hat{Q}_i = \lceil Q_i / \delta_Q \rfloor, \quad \delta_Q = \max(|Q_i|) / 127, \quad \hat{K}_j = \lceil K_j / \delta_K \rfloor, \quad \delta_K = \max(|K_j|) / 127$$

$$S_{ij} = Q_i K_j^\top * \delta_Q * \delta_K$$

Where Q_i, K_j are the tilled block in FlashAttention, and mean(K) is the average value of the channel dimension of K. Additionally, SageAttention keeps $\widetilde{P}V$ as FP16 and uses FP16 Matmul with an FP16 accumulator for $\widetilde{P}V$. However, FP16 Matmul with an FP16 accumulator only has a speedup effect on RTX4090 and RTX3090 GPUs.

3 SageAttention-2

3.1 Formulation

Based on the introduction of FlashAttention and quantization presented in Section 2, we now describe the quantized attention approach we developed.

Quantization:
$$(\delta_Q, \hat{Q}, \overrightarrow{Q}_m) = \phi_Q(Q), \quad (\delta_K, \hat{K}) = \phi_K(K), \quad (\delta_V, \hat{V}, \overrightarrow{V}_m) = \phi_V(V)$$

$$\Delta S = \overrightarrow{Q_m} K^{\top} \tag{2}$$

Attention:
$$S = \psi_{\delta_Q \delta_K}^{-1}(\hat{Q}\hat{K}^{\top}) + \Delta S$$
, $(m', \tilde{P}) = \tilde{\sigma}(m, S)$, $(\delta_P, \hat{P}) = \psi_P(\tilde{P})$

$$O = \operatorname{diag}\left(\exp(m' - m)\right)O + \psi_{\delta_P \delta_V}^{-1}(\hat{P}\hat{V})$$
(3)

 ϕ_Q , ϕ_K , ϕ_V are three transformations to obtain quantized Q, K, and V, which we will discuss in subsequent sections. For simplicity, we omit all superscripts and subscripts, but the matrices used in attention are still tiles, and the computation is still organized as FlashAttention described in Section 2.1. Compared to the original full-precision version, as shown in Eq. 2, 3, SageAttention2 adds quantizers to Q, K, P, V and dequantizers to the product to accelerate both Matmuls of QK and $\widetilde{P}V$.

3.2 Smooth Q

The representative range for quantization of INT4 is notably restrictive, i.e., only $2^4 - 1 = 15$ values. This limitation significantly degrades performance when quantizing Q, K into INT4 in attention. For example,

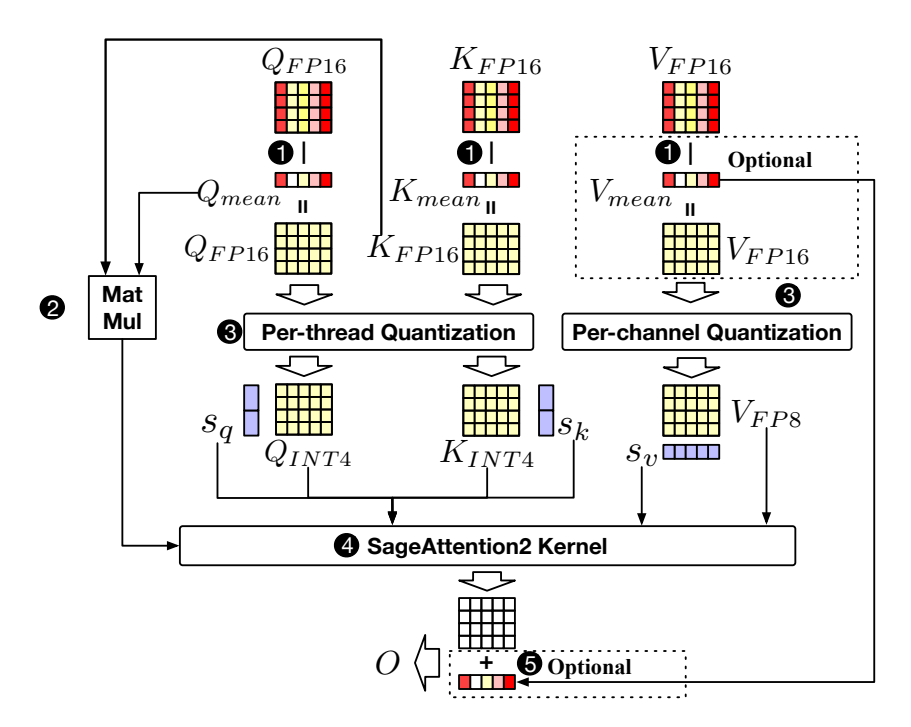


Figure 3: Workflow of SageAttention2. ① Smooth Q,K,V. ② A GEMV to obtain ΔS . ③ Per-thread quantize Q,K and per-channel quantize V. ④ Perform the SageAttention2 kernel. ⑤ Correct the output.

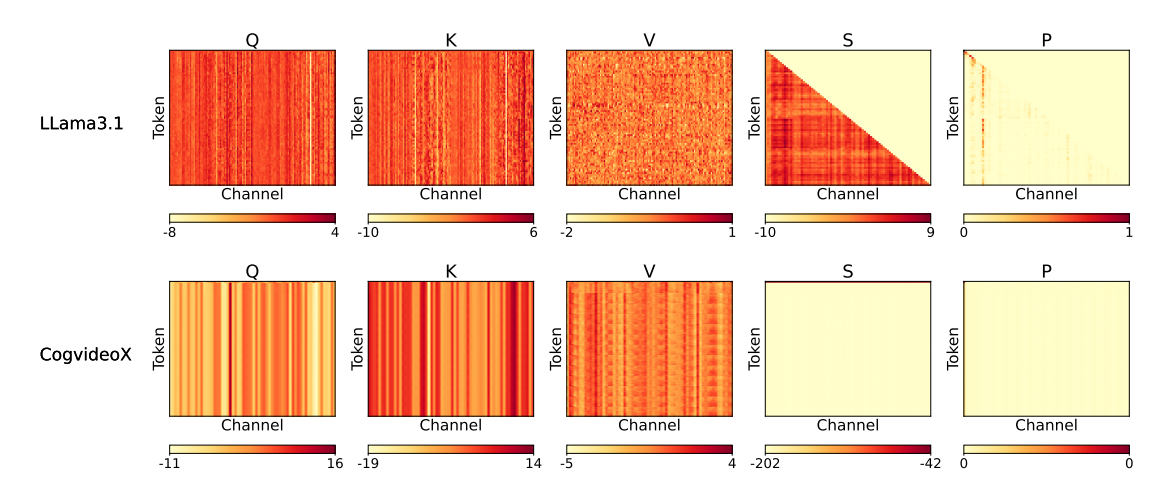


Figure 4: Typical examples of tensors' data distribution in attention.

using INT4 to quantize Q, K can cause the perplexity of Llama3.1 on WikiText to increase by more than 90%, and the quality of videos generated by CogvideoX decrease about 3x (See Table 1). We analyze the data distribution of Q, K in real models. For example, we find that Llama3.1 and CogvideoX show distinct channel-wised outliers in Q, K (See Figure 4). While per-channel quantization could mitigate the quantization error caused by such outliers, this method is impracticable for Q, K because quantization must be conducted along the outer axis (token dimension) of QK^{\top} .

To address this challenge, we propose a method to eliminate the quantization error brought by the outliers in Q, K:

Table 1: End-to-end metrics comparison of different quantization methods, where Q, K are quantized into INT4, while \tilde{P}, V stay in full precision.

Q, K	Smoothing (Q+K)	$egin{array}{c} ext{Llama3.1} \ ext{(Lambda)} \end{array}^{\uparrow}$	$egin{array}{c} ext{Llama3.1} \ ext{(WikeText)} \end{array}^{\downarrow}$	$egin{array}{c} \operatorname{CogVideoX} \ (\operatorname{vqa-a}) \end{array} \uparrow$	$egin{array}{c} \operatorname{CogVideoX} \ (\operatorname{vqa-t}) \end{array} \uparrow$
Full-Precision	-	81.5%	6.013	77.605	75.360
INT4 Quantization	X	72.6%	11.698	27.114	24.670
11114 Quantization	✓	80.8%	6.219	77.276	75.147

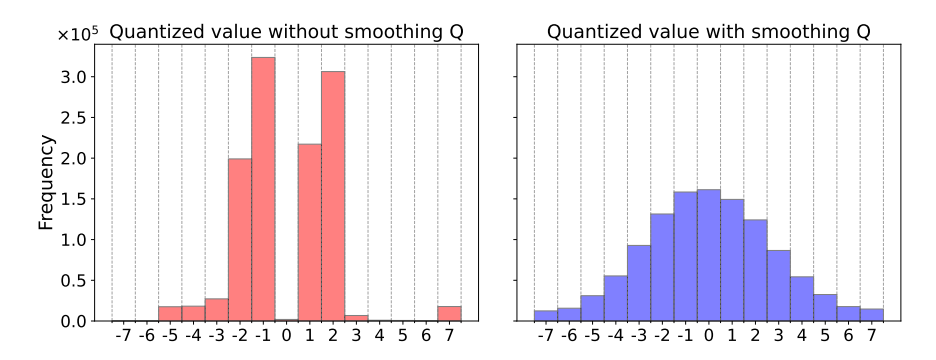


Figure 5: An example of quantized value distribution of Q before and after smoothing Q.

$$\overrightarrow{Q_m} = \operatorname{mean}(Q), \quad \gamma(Q) = Q - \overrightarrow{Q_m}, \quad \gamma(K) = K - \operatorname{mean}(K),$$

$$S = QK = \gamma(Q)\gamma(K) + \overrightarrow{Q_m}\gamma(K)$$

$$\phi_Q(Q) = \psi_Q \circ \gamma(Q), \quad \overrightarrow{Q_m}, \qquad \phi_K(K) = \psi_K \circ \gamma(K)$$

$$(4)$$

Where mean(K) and $\gamma(K)$ have been discussed in SageAttention (Zhang et al., 2024), and the transformation for K does not change the attention score \widetilde{P} . mean(Q) = $\frac{1}{N}\sum_{t=1}^{N}Q[t,:]$ is a vector with a shape $1\times d$. For the transformation of Q, we will perform a GEMV (general matrix-vector multiplication) between \overrightarrow{Q}_m and K^{\top} , i.e., $\overrightarrow{Q}_mK^{\top}$ as ΔS . This ΔS will be added to S during the attention computation. Finally, the transformation from full-precision Q, K to quantized \hat{Q} , \hat{K} can be expressed as shown in Eqution 4, where ψ_Q , ψ_K is two quantizers for Q and K. In other words, full-precision Q, K are substracted with the means of the channel dimension before being quantized.

Figure 5 shows an example from CogvideoX of the distribution of quantized Q with and without smoothing Q. We can find that with smoothing Q, the range of INT4 is utilized more uniformly and fully. Table 1 presents end-to-end metrics for different quantization methods with and without $smoothing\ Q+K$ on Llama3.1 (Dubey et al., 2024) and CogvideoX (Yang et al., 2024). The results demonstrate that $smoothing\ Q+K$ offers significant accuracy benefits. Also, Table 8 and Table 9 show that the order of effectiveness is $smoothing\ Q+K>smoothing\ Q>smoothing\ K>other\ baselines$.

3.3 INT4 Per-thread Quantization

SageAttention uses per-block quantization, which quantizes each block of Q and K for a GPU streaming processor. Such a quantization strategy could achieve an accuracy performance close to per-token quantization.

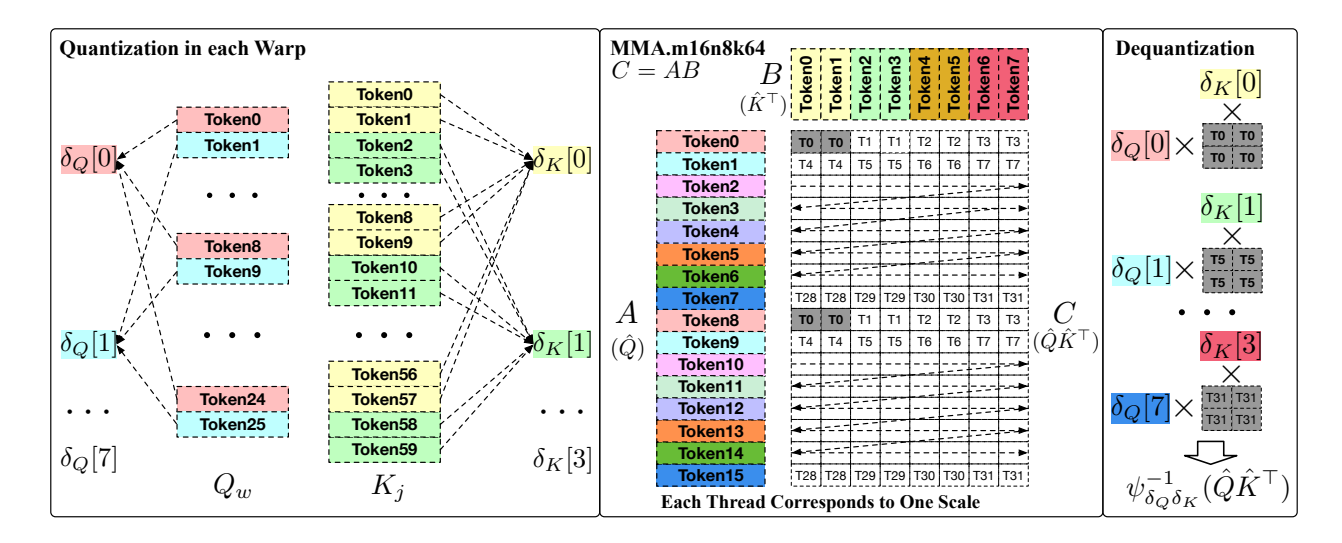


Figure 6: An example of per-thread quantization. The left figure shows the correspondence between the quantization scales and the tokens in each GPU warp. The right figure shows the correspondence between quantization tokens and GPU threads in a MMA.m16n8k64 instruction, showing that each GPU thread only corresponds to one quantization scale in δ_Q and δ_K in dequantization.

Table 2: Average accuracy across all layers of CogvideoX using different quantization granularities.

Table 3:	\mathbf{Worst}	accuracy	${ m across}$	all	layers	of
CogvideoX	using di	fferent quan	tization	gra	nulariti	es.

Per-token	99.45%	0.0649	0.0335			
Per-thread	99.45 %	0.0622	0.0313			
Per-block	98.03%	0.1492	0.0744			
Per-tensor	97.15%	0.1800	0.0865			

Method	Cos Sim ↑	Relative L1 \downarrow	$\mathbf{RMSE}\downarrow$
Per-token	96.76%	0.1916	0.0775
Per-thread	96.72%	0.1932	0.0776
Per-block	90.68%	0.3615	0.1490
Per-tensor	85.85%	0.4687	0.2261

zation and avoid the overhead of the dot product of the quantization scale vectors δ_Q and δ_K . However, quantizing Q and K to INT4 demands a more accurate quantization granularity. We propose per-thread quantization, a more precise and granular quantization approach than the per-block quantizer, also without the additional overhead of vectors dot product required for per-token quantization.

Specifically, each block of Q, i.e., Q_i , in SageAttention will be split into c_w segments and processed by c_w GPU warps in a GPU streaming processor (SM). We call each segment of Q_i as Q_w , and $k_w = K_j$ because a K_j only corresponds to one warp. Then, each warp containing 32 threads uses the mma.m16n8k64 PTX instruction (NVIDIA) for the $Q_wK_j^{\top}$. According to the layout requirement of this instruction, we find that the $Q_w[8 \times (n\%8)]$ could share one quantization scale, and $K_j[8 \times (n\%8)]$ and $K_j[8 \times (n\%8+1)]$ could share one quantization scale, where n is the token index. Such a quantization method is more fine-grained and with no additional overhead. This is because it assigns different GPU threads to distinct quantization groups based on the MMA instruction layout, with each thread performing dequantization only using a single quantization scale value. The per-thread quantization process can be formulated as follows.

$$i_{\delta q} = \lfloor (n * 8 * c_w/b_q) \rfloor$$

$$q_i[i_{\delta q}] = \{8 \times (n\%8) + \lfloor (n * c_w/b_q) \rfloor * b_q/c_w \}, \quad n \in [0, N]$$

$$\delta_Q[i_{\delta q}] = \frac{\max(|Q[q_i[i_{\delta q}]]|)}{7}$$

$$\hat{Q}[q_i[i_{\delta q}]] = \left\lceil \frac{Q[q_i[i_{\delta q}]]}{\delta_Q[i_{\delta q}]} \right\rceil$$

$$i_{\delta k} = \lfloor (n * 4/b_k) \rfloor$$

$$k_n[i_{\delta k}] = \{8 \times (n\%8) + \lfloor n/b_k \rfloor * b_k \} \cup \{8 \times (n\%8) + 1 + \lfloor n/b_k \rfloor * b_k \}, \quad n \in [0, N]$$

$$\delta_K[i_{\delta k}] = \frac{\max(|K[k_n[i_{\delta k}]]|)}{7}$$

$$\hat{K}[k_n[i_{\delta k}]] = \left\lceil \frac{K[k_n[i_{\delta k}]]}{\delta_K[i_{\delta k}]} \right\rceil$$
(6)

We show an example of per-thread quantization in Figure 6.

Algorithm 1 Implementation of SageAttention2.

```
Input: Matrices Q(\text{FP16}), K(\text{FP16}), V(\text{FP16}) \in \mathbb{R}^{N \times d}, block size b_q, b_{kv}, warp count c_w.
Preprocessing: K = K - \text{mean}(K), \ \overrightarrow{Q}_m = \text{mean}(Q), \ Q = Q - \overrightarrow{Q}_m, \ \Delta S = \text{GEMV}(\overrightarrow{Q}_m, K^\top).
Quantization: (\delta_Q, \hat{Q}) = \psi_Q(Q), (\delta_K, \hat{K}) = \psi_K(K). //per-thread. (\delta_V, \hat{V}) = \psi_V(V). //per-channel.
Divide \hat{Q} to T_m = N/b_q blocks \{\hat{Q}_i\}; divide \hat{K}, \hat{V}, and \Delta S to T_n = N/b_{kv} blocks \{\hat{K}_i\}, \{\hat{V}_i\}, and \{\Delta S_i\};
for i = 1 to T_m do
    Load Q_i and \delta_Q = \delta_Q[c_w * 8i : c_w * 8(i+1)] into an SM;
    for j in [1, T_n] do
        Load \hat{K}_j, \hat{V}_j, and \delta_K = \delta_K[4j:4(j+1)] into the SM;
       w = \operatorname{range}(c_w), st = w * c_w

S_i^j[st:st+c_w] = \psi_{\delta_Q\delta_K}^{-1}(\operatorname{Matmul}(\hat{Q}_i[st:st+c_w], \hat{K}_j^{\top})) + \Delta S_j; // Paralleled by c_w warps. The dequantization \psi_{\delta_Q\delta_K}^{-1} is illustrated in Figure 6.
        m_i^j = \max(m_i^{j-1}, \operatorname{rowmax}(S_i^j)), \ \ \widetilde{P}_i^j = \exp(S_i^j - m_i^j), \ \ l_i^j = e^{m_i^{j-1} - m_i^j} + \operatorname{rowsum}(\widetilde{P}_i^j) \ ;
       \begin{split} O_{i}^{j}(\text{FP22}) &= \text{Matmul}((\widetilde{P}_{i}^{j} * 448).\text{to}(\text{FP8.e4m3}), V_{j}) \; ; \\ O_{i}^{j}(\text{FP32}) &= \text{diag}(e^{m_{i}^{j-1} - m_{i}^{j}})^{-1}O_{i}^{j-1}(FP32) + O_{i}^{j}(\text{FP22}) \; ; \end{split}
    end for
    Load \delta_V into an SM;
    O_i = \text{diag}(l_i^{T_n})^{-1} O_i^{T_n}(\text{FP32}) / 448 * \delta_V ;
    Write O_i;
end for
O = \{O_i\}
return O
```

Table 4: Error of the FP8 Matmul instruction of mma(f8f8f32).

Precision of Accumulated Value	E8M13	E8M23	
Error compared to FP32	0	mma(f32.f16.f16.f32) - mma(f32.f8.f8.f32)	

3.4 FP32 MMA Buffer for FP22 Accumulator

To avoid the drawback of SageAttention where FP16 Matmul with an FP16 accumulator for PV is only effective on GPUs such as the RTX4090, we adopt the approach of quantizing P and V to FP8 to leverage the universal acceleration of FP8 Tensor cores. However, we discover that the accumulator for the mma(f32f8f8f32) instruction on the Ada architecture is actually FP22, specifically with 1 sign bit, 8 exponent bits, and 13 mantissa bits. Specifically, for mma (f32f8f8f32) instruction C = AB + D, where A, B are tensors in FP8 data type and C, D are tensors with FP32 data type, we initialize the A, B to zero and vary D to test the data type of the accumulator. As shown in Table 4, when D is initialized with 1 sign bit, 8 exponent bits, and 13 mantissa bits, the value of C matches the result of the mma(f16f16f32) instruction. However, when D is initialized with more than 13 mantissa bits, the error of C corresponds to the difference between the results of mma(f32f16f16f32) and mma(f32f8f8f32). Consequently, the matrix multiplication of PV, quantized to FP8, incurs a certain degree of accuracy loss compared to using an FP32 accumulator.

To mitigate this accuracy loss as much as possible, we propose to use an FP32 buffer to accumulate the values of $P_i^j V_j$ in FP22. Specifically, as shown in Algorithm 1, after each Matmul between the tiled P and V, we store the Matmul result in the FP32 buffer. This approach prevents the FP22 accumulator from accumulating errors across the entire sequence, confining errors to the tiled range instead.

Table 5: Average accuracy using different data Table 6: Worst accuracy using different data types types of (P,V) across all layers of a CogvideoX of (P,V) across all layers of a CogvideoX model, model, where (Q, K) are smoothed.

Q, K	\widetilde{P}, V	Cos Sim ↑	Relative L1 \downarrow	$ ho$ RMSE \downarrow
	INT8	77.05%	0.5618	0.5044
INT4	E5M2	99.20%	0.0905	0.0903
111 1 4	E4M3	99.44%	0.0683	0.0347
	FP16	99.45%	0.0649	0.0335

where (Q, K) are smoothed.

Q, K	$ \widetilde{P}, V$	Cos Sim ↑	Relative L1 \downarrow	$ \mathbf{RMSE}\downarrow$
	INT8	19.52%	0.9579	1.4483
INT4	E5M2	94.94%	0.2327	0.2361
11114	E4M3	96.70%	0.1956	0.0779
	FP16	96.76%	0.1916	0.0775

Table 7: Two kernel implementations of SageAttention2.

Kernel	$\psi_Q(Q),\psi_K(K)$	$\psi_P(\widetilde{P}),\psi_V(V)$
SageAttn2-4b	INT4, per-thread	FP8, per-block; FP8, per-channel
SageAttn2-8b	INT8, per-thread	FP8, per-block; FP8, per-channel

Quantization for Q, K, P, V 3.5

Quantization for Q, K. We propose $\psi_Q(Q)$ and $\psi_K(K)$ in granularity of per-thread. This is first because per-channel quantization is not feasible since the scale factors of the inner axis of QK^{\top} cannot used to do dequantization (Xiao et al., 2023a). Second, as shown in Table 2 and Table 3, we compare the average and worst-case accuracies of INT4 quantization at per-token, per-thread, per-block, and per-tensor granularity using real Q, K, V across all layers of Cogvideox. Results indicate that the accuracy of per-thread quantization is very close to per-token and outperforms a lot more than per-block and per-tensor. Furthermore, per-thread quantization incurs less dequantization overhead than per-token, as discussed in Section 3.3.

Quantization for P, V. We choose FP8, specifically the E4M3 data type, for $\psi_P(P)$ and $\psi_V(V)$ for two reasons. First, most GPUs have tensor cores that support FP8 Matmul operations, which are twice as fast as those using FP16. Second, Table 5 and Table 6 show the average and worst accuracy of different data types used for P, V using real Q, K, V across all layers of CogvideoX. We can see that the accuracy of using E4M3 is very close to that of using FP16 and superior to that of E5M2 and INT8. We propose to use $\psi_P(P)$ in per-block and $\psi_V(V)$ in per-channel for three reasons. First, per-channel quantization for P and per-token quantization for V are not viable because dequantization requires scale factors of outer axis.

Second, $\widetilde{P} = \exp(S_i - \operatorname{rowmax}(S_i))$, where S_i is the Matmul result of a block of Q and K^{\top} , the max value in each row of \widetilde{P} is 1. Hence, we can assign a single static scale $s = \frac{1}{448}$ to a block \widetilde{P} . Third, per-channel quantization can address the channel-wised outlier of V.

Accuracy metrics. We use three metrics to assess the accuracy of quantized attention output O' compared to attention output in full-precision O: First, we flatten O' and O into vectors in the shape of $1 \times n$. Then, Cosine similarity: $CosSim = \sum OO'/\sqrt{\sum O^2}\sqrt{\sum O'^2}$, Relative L1 distance: $L1 = \sum |O-O'|/\sum |O|$, Root mean square error: $RMSE = \sqrt{(1/n)\sum(O-O')^2}$.

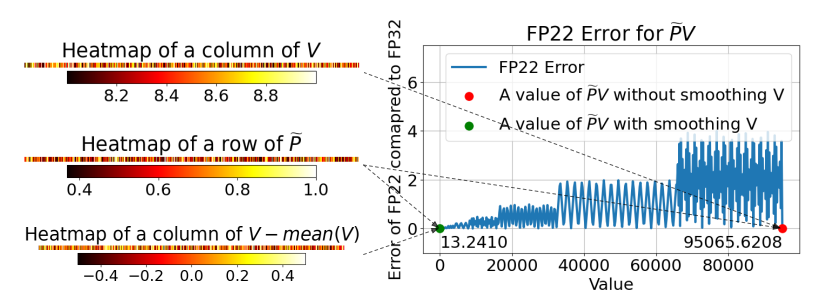


Figure 7: An example of dot product precision a row of \widetilde{P} and a column of V presented by FP22 data type.

3.6 An Optional Technique: Smooth V

We also figure out another way to mitigate the accuracy loss due to the FP22 accumulator when V possesses channel-wise biases:

$$\gamma(V) = V - \text{mean}(V), \quad \text{mean}(V) = \overrightarrow{V_m}$$

$$\phi_V(V) = \psi_V \circ \gamma, \ \overrightarrow{V_m}$$
(7)

As shown in Figure 7, this strategy could enhance the accuracy of FP22 for values in $\widetilde{P}V$ for the following reasons: Each row of \widetilde{P} spans a value range from 0 to 1, and each column of V consistently features channelwise biases that are exclusively positive or negative, for instance, ranging between 8 and 9. Consequently, the values of $\widetilde{P}V$ could be quite large. However, the floating-point number representation range is not uniform—it is denser near zero. Therefore, by subtracting the mean along the channel dimension from V, the values of $\widetilde{P}V$ will be closer to zero, resulting in higher representational precision. We believe such an explanation and strategy could address lots of issues reported by the community. Additionally, to maintain the correctness of the attention computation, it is only necessary to add $\overrightarrow{V_m}$ to the final calculation of O: $O = O + \overrightarrow{V_m}$. This is because the sum of each row of the \widetilde{P} matrix equals 1, so $\widetilde{P}\overrightarrow{V_m} = \overrightarrow{V_m}$. In other words, this method decomposes V into two parts: $\overrightarrow{V_m}$ and V. For V, it centers the values of each column around zero, which leads to the dot product result between a row from the quantized \widetilde{P} matrix and a column from the quantized V matrix being closer to zero. This makes the representation of FP22 more accurate. Meanwhile, $\overrightarrow{V_m}$ is retained in FP16 and added to O at the end without causing a loss of precision for the $\overrightarrow{V_m}$ part.

Remark. This technique is optional and not employed in our main experiments. This is because its benefits are marginal, only significantly enhancing attention accuracy primarily when V exhibits channel-wise outliers, which are absent in some models, such as V in Llama3.1 (see Figure 4).

https://github.com/triton-lang/triton/issues/4476, https://github.com/triton-lang/triton/issues/5065

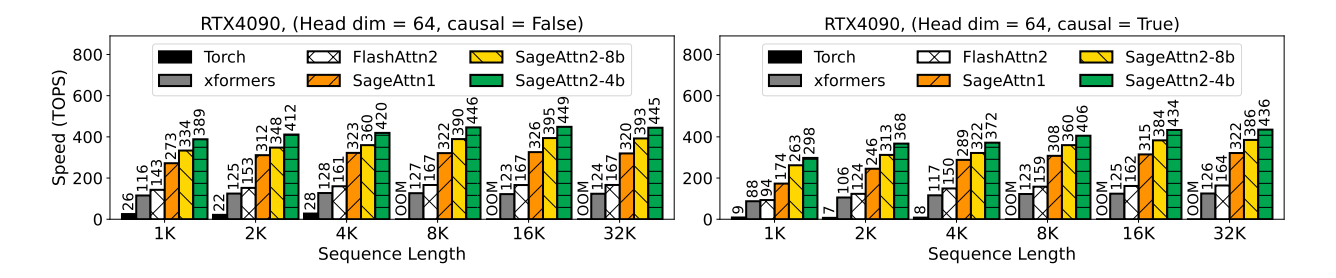


Figure 8: Speed comparison between SageAttention2 and baselines (RTX4090, headdim=64).

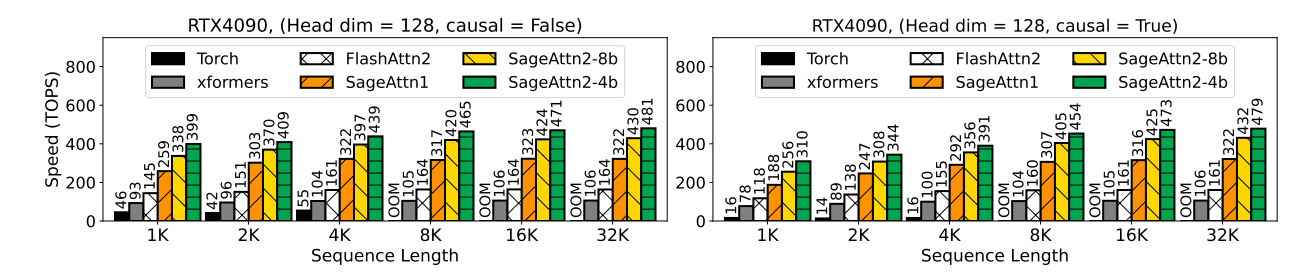


Figure 9: Speed comparison between SageAttention2 and baselines (RTX4090, headdim=128).

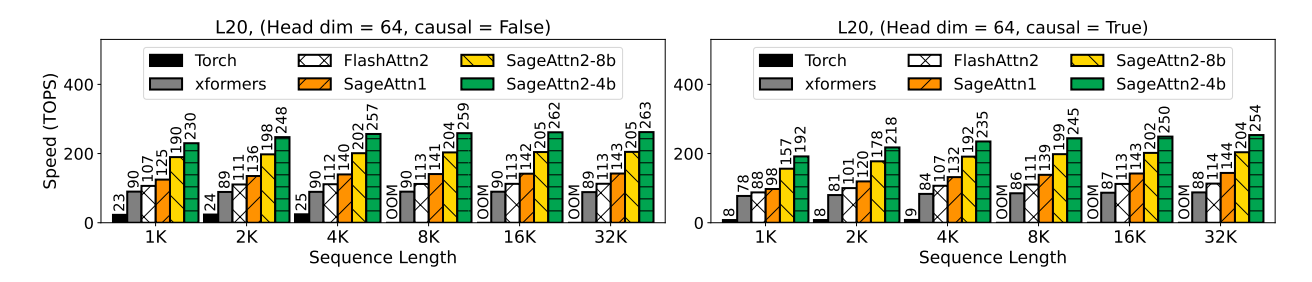


Figure 10: Speed comparison between SageAttention2 and baselines (L20, headdim=64).

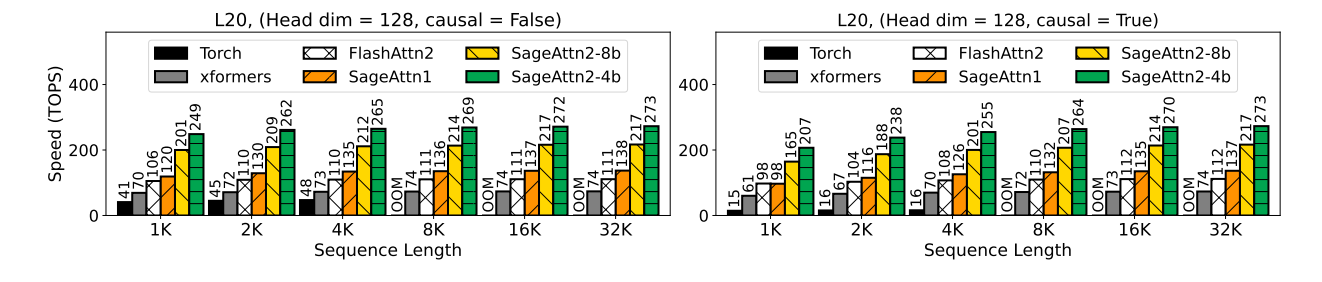


Figure 11: Speed comparison between SageAttention2 and baselines (L20, headdim=128).

4 Experiment

4.1 Setup

Models. We validate the effectiveness of SageAttention2 across a diverse set of representative models from language, image, and video generation. Specifically, we conduct experiments on ten models:

Llama2 (7B) (Touvron et al., 2023), Llama3.1 (8B) (Dubey et al., 2024), and GLM4 (9B) (GLM et al., 2024) for text2text, CogvideoX (2B), CogvideoX (1.5-5B) (Yang et al., 2024), HunyuanVideo (Weijie Kong & Jie Jiang, 2024), and Mochi (Team, 2024) for text2video, Flux (schnell) (Black Forest Labs, 2023) and Stable-Diffusion3.5 (turbo) (Stability AI, 2023) for text2image, and TIMM (Wightman, 2019) for image classification.

Datasets. Text-to-text models are evaluated on four zero-shot tasks: WikiText (Merity et al., 2022) to assess the model's prediction confidence, LAMBADA (Paperno et al., 2016) evaluate contextual understanding, MMLU (Hendrycks et al., 2020) for measuring knowledge across various subjects, and Longbench (Bai et al., 2023) for evaluating bilingual, multitask, and comprehensive assessment of long context understanding capabilities. Text-to-video models are evaluated using the open-sora (Zheng et al., 2024) prompt sets. Text-to-image models are assessed on MJHQ-30K (Li et al., 2024). TIMM is evaluated on on three image datasets: ImageNet (Deng et al., 2009), ImageNet-Sketch (Sketch) (Wang et al., 2019), and ImageNet-Rendition (ImageNet-r) (Hendrycks et al., 2021).

Metrics. For text-to-text models, we use perplexity (ppl.) (Jelinek et al., 1977) for WikiText, Accuracy (Acc.) for LAMBADA and MMLU, and Longbench score (Bai et al., 2023). For text-to-video models, following Zhao et al. (2024), we evaluate the quality of generated videos on five metrics: CLIPSIM and CLIP-Temp (CLIP-T) (Liu et al., 2024) to measure the text-video alignment; (VQA-a) and (VQA-t) to assess the video aesthetic and technical quality, respectively; and Flow-score (FScore) for temporal consistency (Wu et al., 2023). For text-to-image models, generated images are compared with the images in MJHQ-30K dataset in three aspects: FID (Heusel et al., 2017) and sFID (Salimans et al., 2016) for fidelity evaluation, Clipscore (CLIP) (Hessel et al., 2021) for text-image alignment, and ImageReward (IR) (Xu et al., 2024) for human preference. For TIMM, we use classification accuracy.

Implemetation details. We implement our attention kernels using CUDA and conduct experiments on Ubuntu 22.04 servers with RTX4090 and L20 GPUs.

Baselines. (1) SmoothAttn. Following Qserve (Lin et al., 2024), we apply smooth quant for matrixes Q, K with smoothing factor $\alpha = 0.5$. (2) HadmdAttn. Following Quarot (Ashkboos et al., 2024), we apply random Hadamard transformation for matrixes Q, K before INT4 quantization. (3) SageAttention (Zhang et al., 2024) uses smoothing K, INT8 per-block quantization for Q, K, and FP16 for \tilde{P}, V .

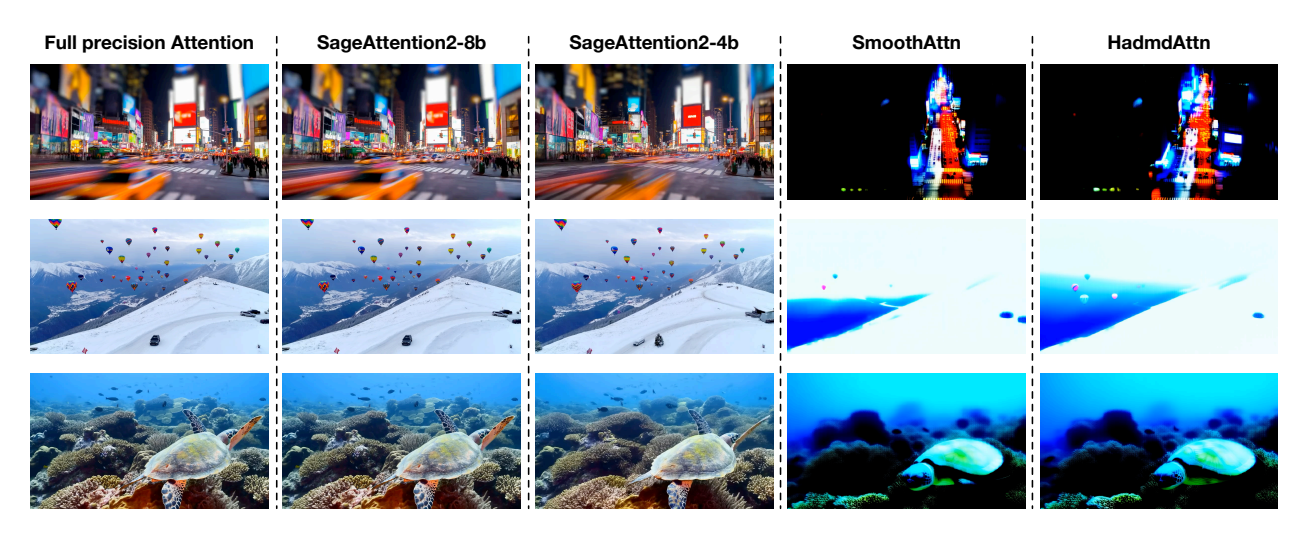


Figure 12: Comparison examples from HunyuanVideo, prompts are sampled from open-sora prompt sets.

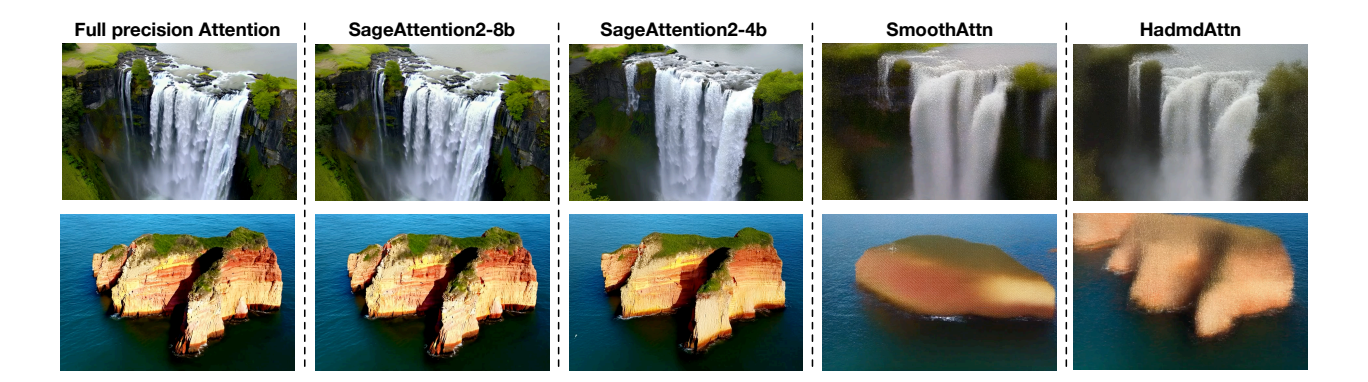


Figure 13: Comparison examples from CogvideoX (2B), prompts are sampled from open-sora prompt sets.

CogvideoX using different smooth methods.

Method	$\mathbf{CosSim} \uparrow$	Relative L1 \downarrow	$ \mathbf{RMSE} \downarrow$
None	80.04%	0.3906	0.2223
HadmdAttn	79.77%	0.3782	0.2180
SmoothAttn	90.21%	0.3383	0.1952
Smooth K (Ours)	98.07%	0.1493	0.0743
Smooth Q (Ours)	98.30%	0.1250	0.0712
SageAttn2-4b	99.46%	0.0648	0.0334

Table 8: Average accuracy across all layers of Table 9: Worst accuracy across all layers of CogvideoX using different smooth methods.

Method	CosSim ↑	Relative L1 \downarrow	$ \mathbf{RMSE}\downarrow$
None	4.83%	0.9979	0.7784
HadmdAttn	4.85%	0.9978	0.7785
${\tt SmoothAttn}$	64.49%	0.9262	0.7204
Smooth K (Ours)	90.86%	0.3565	0.1464
Smooth Q (Ours)	93.10%	0.2989	0.2195
SageAttn2-4b	96.71%	0.1956	0.0779

4.2 Speed and Accuracy of Kernels

Speed. We conduct experiments to compare the Speed of SageAttention2 against baselines using configurations with headdim=64 and headdim=128, both with and without Causal Mask (Vaswani, 2017). Specifically, Figure 8 and Figure 9, show the speed of SageAttention2 and baselines across varying sequence lengths on RTX4090. These results indicate that SageAttn2-4b and SageAttn-8b are approximately 3x and 2.7x faster than FlashAttention2, and about 4.5x and 4x faster than xformers, respectively.

Accuracy. Table 8 and Table 9 show that the average and worst accuracy of different methods with INT4 Q, K and FP8 P, V across all layers of CogvideoX. The results indicate that the accuracy of SageAttn-4b is superior to other baselines.

End-to-end Performance 4.3

Metrics loss. We assessed the end-to-end metrics of various models using SageAttention2 compared to using attention in full precision. Detailed evaluation results are presented in Table 10 for Llama2, Llama3.1, GLM4, CogvideoX (2B), CogvideoX (1.5-5B), HunyuanVideo, Mochi, Flux, Stable-Diffusion3.5, and TIMM, respectively. The results indicate that SageAttn-4b outperforms all baselines and maintains most of the endto-end accuracy across all models. Additionally, SageAttn-8b incurs almost no metrics loss across various models.

Visible examples. Figure 12 and Figure 13 show some visible comparision examples from Hunyuan Video and CogvideoX (1.5-5B). We can observe that SageAttn-8b does not introduce any visible differences compared to full-precision attention, whereas SageAttn-4b has minor differences compared to full-precision attention but is much better than the baselines.

End-to-end speedup. We compared the original generation latency and the latency using SageAttention2

Table 10: End-to-end metrics across text and video generation models. - means the model does not support this dataset evaluation. \boldsymbol{X} indicates an inability to generate results for evaluation.

Model		WikiText (Ppl.)	↓ Lambda (A	cc.) † MMI	LU (Acc.) ↑	$\textbf{Longbench} \uparrow$
	Full-Precision	5.823	0.886		0.439	-
	HadmdAttn	6.771	0.860		0.360	-
Llama2	SmoothAttn	6.717	0.867		0.392	-
Lialiaz	SageAttn-4b	$\bf 5.912$	0.881	0.881		-
	SageAttn-8b	$\bf 5.828$	0.886		0.438	-
	SageAttention	$\bf 5.824$	0.887		0.439	-
	Full-Precision	6.013	0.815		0.635	49.40
	HadmdAttn	7.872	0.762		0.500	44.07
Llama3.1	SmoothAttn	7.180	0.783		0.541	44.69
LIamas.1	SageAttn-4b	$\boldsymbol{6.256}$	0.798		0.607	48.79
	SageAttn-8b	6.019	0.811		0.634	49.59
	SageAttention	6.017	0.812		0.634	49.55
	Full-Precision	7.241	0.432		0.743	49.78
	HadmdAttn	7.989	0.435		0.669	45.97
GLM4	SmoothAttn	8.943	0.449		0.592	42.20
GLM4	SageAttn-4b	7.352	0.433		0.725	49.23
	SageAttn-8b	7.242	0.432		0.745	49.60
	SageAttention	7.243	0.433		0.744	49.79
Model	Attention	CLIPSIM ↑	CLIP-T↑	VQA-a ↑	VQA-t ↑	FScore ↑
	Full-Precision	0.1836	0.9975	77.605	75.360	3.006
	HadmdAttn	0.1742	0.9877	29.780	23.985	0.499
CogvideoX	SmoothAttn	0.1741	0.9870	41.703	47.043	0.624
(2B)	SageAttn-4b	0.1821	0.9973	77.368	74.906	2.603
()	SageAttn-8b	0.1829	0.9977	76.532	74.281	2.941
	SageAttention	0.1833	0.9976	76.997	71.360	2.988
	Full-Precision	0.1778	0.9979	70.231	70.928	2.507
	HadmdAttn	0.1576	0.9933	8.990	2.299	X
CogvideoX	SmoothAttn	0.1559	0.9950	8.812	2.277	X
(1.5-5B)	SageAttn-4b	0.1721	0.9978	57.729	52.989	2.884
,	SageAttn-8b	0.1775	0.9980	69.492	74.415	2.487
	SageAttention	×	X	X	X	X
	Full-Precision	0.1783	0.9995	82.516	75.934	0.604
	HadmdAttn	0.1727	0.9989	7.514	0.762	0.175
	SmoothAttn	0.1739	0.9988	6.987	0.609	0.148
HunyuanVideo	SageAttn-4b	0.1751	0.9995	81.478	65.371	0.610
	SageAttn-8b	0.1782	0.9996	81.786	75.354	0.586
	SageAttention	0.1786	0.9995	82.496	79.843	0.597
	Full-Precision	0.1798	0.9986	45.549	65.416	1.266
	HadmdAttn	0.1733	0.9980	9.053	25.133	0.704
	SmoothAttn	0.1687	0.9978	3.383	3.480	0.241
Mochi	SageAttn-4b	0.1783	0.9986	35.955	43.735	1.137
	SageAttn-8b	0.1797	0.9986	46.760	64.901	1.255
	SageAttention	0.1800	0.9987	48.707	63.763	1.269

for models with long sequence lengths in Table 12, observing significant speedup effects. For instance, SageAttention2 achieved a 1.8x speedup in CogvideoX (1.5-5B) without any metrics loss (SageAttn-8b).

Table 11: Table 10 continued. End-to-end metrics across image generation and classification models.

Model	Attention	$\mathbf{FID}\downarrow$	$\mathbf{sFID}\downarrow$	CLIP ↑	IR ↑
	Full-Precision	10.960	16.648	26.180	1.009
	HadmdAttn	11.353	18.495	26.123	0.965
P1	SmoothAttn	11.149	19.017	26.109	0.959
Flux	SageAttn-4b	10.577	17.497	26.141	0.998
	SageAttn-8b	10.927	16.723	26.175	1.009
	SageAttention	10.944	16.641	26.171	1.008
	Full-Precision	14.105	15.646	25.505	0.902
	HadmdAttn	14.259	15.909	25.513	0.886
Stable-Dif	SmoothAttn	14.161	15.649	25.510	0.887
fusion3.5	SageAttn-4b	14.097	15.397	25.487	$\boldsymbol{0.895}$
	SageAttn-8b	14.106	15.647	25.499	0.901
	SageAttention	14.140	15.678	25.503	0.902

Model	Attention	ImageNet (Acc.) ↑	Sketch (Acc.) \uparrow	ImageNet-r (Acc.) \uparrow
TIMM	Full-Precision	84.79%	45.32%	59.55%
	HadmdAttn	84.50%	44.89%	58.80%
	SmoothAttn	84.40%	44.68%	58.73%
	SageAttn-4b	86.67%	45.24%	59.29 %
	SageAttn-8b	84.79%	45.39%	59.57 %
	SageAttention	84.74%	45.38%	59.95 %

Table 12: End-to-end generation latency using SageAttention2 (The latency of Llama3.1 is the time to first token generation using different sequence lengths).

Model	GPU	Original	SageAttn-8b	SageAttn-4b
${\tt CogvideoX}\;(2B)$	RTX4090	86 s	54 s	52 s
${ t CogvideoX} \ (1.5{ t -}5{ t B})$	RTX4090	$1040 {\rm \ s}$	577 s	$555 \mathrm{\ s}$
HunyuanVideo	L20	$2221 \mathrm{\ s}$	$1486 \mathrm{\ s}$	$1435 \mathrm{\ s}$
Mochi	L20	$2336 \mathrm{\ s}$	$1316 \mathrm{\ s}$	1190 s
Llama3.1 $(48K \text{ tokens})$	RTX4090	$9.2 \mathrm{\ s}$	5.7 s	5.6 s
Llama3.1 $(100K \text{ tokens})$	L20	$39.9 \mathrm{\ s}$	25.4 s	23.2 s

 ${\tt SageAttn-4b} \ {\tt further} \ {\tt accelerated} \ {\tt these} \ {\tt models} \ {\tt but} \ {\tt with} \ {\tt a} \ {\tt little} \ {\tt metrics} \ {\tt loss}.$

Table 13: An accuracy example on real tensors of CogvideoX model with or without smoothing V.

Smooth V	Cos Sim ↑	Relative L1 \downarrow	\mid RMSE \downarrow
X	98.25%	0.1980	0.2387
\checkmark	99.75%	0.0406	0.0773

4.4 Ablation Study

Overhead of smoothing Q, K. Note that the overhead of smoothing Q, K only contains $Q - \overrightarrow{Q_m}$, K - mean(K), and $\overrightarrow{Q_m}K^{\top}$. The speed overhead of smoothing Q, K accounts for about 3.5% of the attention

kernel.

Benefit of smoothing V. Table 13 shows the attention accuracy on real tensors sampled from CogvideoX with and without smoothing V. It demonstrates that smoothing V could improve the accuracy of SageAttention2 when quantizing Q, K to INT4 and \widetilde{P}, V to FP8.

5 Conclusion and Future Work

We introduce SageAttention2, an efficient and accurate quantization method for attention. First, we propose to quantize matrixes (Q,K) to INT4 in a thread-level granularity and quantize matrixes (\tilde{P},V) to FP8. Second, we propose a method to smooth Q, enhancing the accuracy of INT4 QK. Third, we propose to use an FP32 Matmul buffer for PV to enhance the accuracy of FP8 $\tilde{P}V$. Our implementation is faster than FlashAttention2 and xformers by approximately $\mathbf{3x}$ and $\mathbf{5x}$ on RTX4090, respectively. Extensive testing confirms that our approach maintains end-to-end metrics across various models, including language, and video generation.

Future Work. We leave the implementation of FP8 MatMul with an FP16 accumulator for $\widetilde{P}V$ and SageAttention2 on the Hopper architecture for future work.

References

- Ashkboos, S., Mohtashami, A., Croci, M. L., Li, B., Cameron, P., Jaggi, M., Alistarh, D., Hoefler, T., and Hensman, J. Quarot: Outlier-free 4-bit inference in rotated llms, 2024. URL https://arxiv.org/abs/2404.00456.
- Bai, Y., Lv, X., Zhang, J., Lyu, H., Tang, J., Huang, Z., Du, Z., Liu, X., Zeng, A., Hou, L., et al. Longbench: A bilingual, multitask benchmark for long context understanding. arXiv preprint arXiv:2308.14508, 2023.
- Black Forest Labs. Flux. https://github.com/black-forest-labs/flux, 2023.
- Chen, Y., Qian, S., Tang, H., Lai, X., Liu, Z., Han, S., and Jia, J. Longlora: Efficient fine-tuning of long-context large language models. arXiv preprint arXiv:2309.12307, 2023.
- Choromanski, K., Likhosherstov, V., Dohan, D., Song, X., Gane, A., Sarlos, T., Hawkins, P., Davis, J., Mohiuddin, A., Kaiser, L., et al. Rethinking attention with performers. arXiv preprint arXiv:2009.14794, 2020.
- Chu, X., Tian, Z., Wang, Y., Zhang, B., Ren, H., Wei, X., Xia, H., and Shen, C. Twins: Revisiting the design of spatial attention in vision transformers. *Advances in neural information processing systems*, 34: 9355–9366, 2021.
- Dao, T. Flashattention-2: Faster attention with better parallelism and work partitioning. arXiv preprint arXiv:2307.08691, 2023.
- Dao, T., Fu, D., Ermon, S., Rudra, A., and Ré, C. Flashattention: Fast and memory-efficient exact attention with io-awareness. *Advances in Neural Information Processing Systems*, 35:16344–16359, 2022.
- Deng, J., Dong, W., Socher, R., Li, L.-J., Li, K., and Fei-Fei, L. Imagenet: A large-scale hierarchical image database. In 2009 IEEE conference on computer vision and pattern recognition, pp. 248–255. Ieee, 2009.
- Dubey, A., Jauhri, A., Pandey, A., Kadian, A., Al-Dahle, A., Letman, A., Mathur, A., Schelten, A., Yang, A., Fan, A., et al. The llama 3 herd of models. arXiv preprint arXiv:2407.21783, 2024.
- Fu, T., Huang, H., Ning, X., Zhang, G., Chen, B., Wu, T., Wang, H., Huang, Z., Li, S., Yan, S., Dai, G., Yang, H., and Wang, Y. Moa: Mixture of sparse attention for automatic large language model compression, 2024. URL https://arxiv.org/abs/2406.14909.

- Gao, Y., Zeng, Z., Du, D., Cao, S., So, H. K.-H., Cao, T., Yang, F., and Yang, M. Seerattention: Learning intrinsic sparse attention in your llms, 2024. URL https://arxiv.org/abs/2410.13276.
- gkamradt. Llmtest needle in a haystack pressure testing llms. https://github.com/gkamradt/LLMTest_NeedleInAHaystack, 2023.
- GLM, T., Zeng, A., Xu, B., Wang, B., Zhang, C., Yin, D., Rojas, D., Feng, G., Zhao, H., Lai, H., Yu, H., Wang, H., Sun, J., Zhang, J., Cheng, J., Gui, J., Tang, J., Zhang, J., Li, J., Zhao, L., Wu, L., Zhong, L., Liu, M., Huang, M., Zhang, P., Zheng, Q., Lu, R., Duan, S., Zhang, S., Cao, S., Yang, S., Tam, W. L., Zhao, W., Liu, X., Xia, X., Zhang, X., Gu, X., Lv, X., Liu, X., Liu, X., Yang, X., Song, X., Zhang, X., An, Y., Xu, Y., Niu, Y., Yang, Y., Li, Y., Bai, Y., Dong, Y., Qi, Z., Wang, Z., Yang, Z., Du, Z., Hou, Z., and Wang, Z. Chatglm: A family of large language models from glm-130b to glm-4 all tools, 2024.
- Hendrycks, D., Burns, C., Basart, S., Zou, A., Mazeika, M., Song, D., and Steinhardt, J. Measuring massive multitask language understanding. 2020.
- Hendrycks, D., Basart, S., Mu, N., Kadavath, S., Wang, F., Dorundo, E., Desai, R., Zhu, T., Parajuli, S., Guo, M., Song, D., Steinhardt, J., and Gilmer, J. The many faces of robustness: A critical analysis of out-of-distribution generalization. *ICCV*, 2021.
- Hessel, J., Holtzman, A., Forbes, M., Le Bras, R., and Choi, Y. Clipscore: A reference-free evaluation metric for image captioning. In *Proceedings of the 2021 Conference on Empirical Methods in Natural Language Processing*, pp. 7514–7528, 2021.
- Heusel, M., Ramsauer, H., Unterthiner, T., Nessler, B., and Hochreiter, S. Gans trained by a two time-scale update rule converge to a local nash equilibrium. *Advances in neural information processing systems*, 30, 2017.
- Jelinek, F., Mercer, R. L., Bahl, L. R., and Baker, J. K. Perplexity—a measure of the difficulty of speech recognition tasks. *The Journal of the Acoustical Society of America*, 62(S1):S63–S63, 1977.
- Jiang, H., Li, Y., Zhang, C., Wu, Q., Luo, X., Ahn, S., Han, Z., Abdi, A. H., Li, D., Lin, C.-Y., et al. Minference 1.0: Accelerating pre-filling for long-context llms via dynamic sparse attention. arXiv preprint arXiv:2407.02490, 2024.
- Katharopoulos, A., Vyas, A., Pappas, N., and Fleuret, F. Transformers are rnns: Fast autoregressive transformers with linear attention. In *International conference on machine learning*, pp. 5156–5165. PMLR, 2020.
- Lefaudeux, B., Massa, F., Liskovich, D., Xiong, W., Caggiano, V., Naren, S., Xu, M., Hu, J., Tintore, M., Zhang, S., Labatut, P., Haziza, D., Wehrstedt, L., Reizenstein, J., and Sizov, G. xformers: A modular and hackable transformer modelling library. https://github.com/facebookresearch/xformers, 2022.
- Li, D., Kamko, A., Akhgari, E., Sabet, A., Xu, L., and Doshi, S. Playground v2.5: Three insights towards enhancing aesthetic quality in text-to-image generation, 2024.
- Li, K., Wang, Y., Peng, G., Song, G., Liu, Y., Li, H., and Qiao, Y. Uniformer: Unified transformer for efficient spatial-temporal representation learning. In *International Conference on Learning Representations*.
- Lin, Y., Tang, H., Yang, S., Zhang, Z., Xiao, G., Gan, C., and Han, S. Qserve: W4a8kv4 quantization and system co-design for efficient llm serving, 2024. URL https://arxiv.org/abs/2405.04532.
- Liu, Y., Cun, X., Liu, X., Wang, X., Zhang, Y., Chen, H., Liu, Y., Zeng, T., Chan, R., and Shan, Y. Evalcrafter: Benchmarking and evaluating large video generation models. In *Proceedings of the IEEE/CVF Conference on Computer Vision and Pattern Recognition*, pp. 22139–22149, 2024.

- Liu, Z., Lin, Y., Cao, Y., Hu, H., Wei, Y., Zhang, Z., Lin, S., and Guo, B. Swin transformer: Hierarchical vision transformer using shifted windows. In *Proceedings of the IEEE/CVF international conference on* computer vision, pp. 10012–10022, 2021.
- Merity, S., Xiong, C., Bradbury, J., and Socher, R. Pointer sentinel mixture models. In *International Conference on Learning Representations*, 2022.
- Milakov, M. and Gimelshein, N. Online normalizer calculation for softmax. arXiv preprint arXiv:1805.02867, 2018.
- NVIDIA. Parallel thread execution is version 8.5. https://docs.nvidia.com/cuda/parallel-thread-execution/.
- Paperno, D., Kruszewski, G., Lazaridou, A., Pham, N.-Q., Bernardi, R., Pezzelle, S., Baroni, M., Boleda, G., and Fernández, R. The lambada dataset: Word prediction requiring a broad discourse context. In Proceedings of the 54th Annual Meeting of the Association for Computational Linguistics (Volume 1: Long Papers), pp. 1525–1534, 2016.
- Salimans, T., Goodfellow, I., Zaremba, W., Cheung, V., Radford, A., and Chen, X. Improved techniques for training gans. *Advances in neural information processing systems*, 29, 2016.
- Shah, J., Bikshandi, G., Zhang, Y., Thakkar, V., Ramani, P., and Dao, T. Flashattention-3: Fast and accurate attention with asynchrony and low-precision. arXiv preprint arXiv:2407.08608, 2024.
- Stability AI. Introducing stable diffusion 3.5. https://stability.ai/news/introducing-stable-diffusion-3-5, 2023.
- Team, G. Mochi 1. https://github.com/genmoai/models, 2024.
- Touvron, H., Martin, L., Stone, K., Albert, P., Almahairi, A., Babaei, Y., Bashlykov, N., Batra, S., Bhargava, P., Bhosale, S., et al. Llama 2: Open foundation and fine-tuned chat models. arXiv preprint arXiv:2307.09288, 2023.
- Vaswani, A. Attention is all you need. Advances in Neural Information Processing Systems, 2017.
- Venkataramanan, S., Ghodrati, A., Asano, Y. M., Porikli, F., and Habibian, A. Skip-attention: Improving vision transformers by paying less attention. arXiv preprint arXiv:2301.02240, 2023.
- Wang, H., Ge, S., Lipton, Z., and Xing, E. P. Learning robust global representations by penalizing local predictive power. *Advances in Neural Information Processing Systems*, 32, 2019.
- Wang, S., Li, B. Z., Khabsa, M., Fang, H., and Ma, H. Linformer: Self-attention with linear complexity. arXiv preprint arXiv:2006.04768, 2020.
- Weijie Kong, Qi Tian, Z. Z. R. M. Z. D. J. Z. J. X. X. L. B. W. J. Z. K. W. Q. L. A. W. A. W. C. L. D. H. F. Y. H. T. H. W. J. S. J. B. J. W. J. X. J. W. J. Y. K. W. M. L. P. L. S. L. W. W. W. Y. X. D. Y. L. Y. L. Y. C. Y. C. Y. P. Z. Y. Z. H. Z. X. Z. Z. Z. X. Y. T. Q. L. S. L. D. Z. H. W. Y. Y. D. W. Y. L. and Jie Jiang, a. w. C. Z. Hunyuanvideo: A systematic framework for large video generative models, 2024. URL https://arxiv.org/abs/2412.03603.
- Wightman, R. Pytorch image models. https://github.com/rwightman/pytorch-image-models, 2019.
- Wu, H., Zhang, E., Liao, L., Chen, C., Hou, J., Wang, A., Sun, W., Yan, Q., and Lin, W. Exploring video quality assessment on user generated contents from aesthetic and technical perspectives. In *Proceedings* of the IEEE/CVF International Conference on Computer Vision, pp. 20144–20154, 2023.

- Xiao, C., Zhang, P., Han, X., Xiao, G., Lin, Y., Zhang, Z., Liu, Z., and Sun, M. Infllm: Training-free long-context extrapolation for llms with an efficient context memory. In First Workshop on Long-Context Foundation Models@ ICML 2024, 2024.
- Xiao, G., Lin, J., Seznec, M., Wu, H., Demouth, J., and Han, S. Smoothquant: Accurate and efficient post-training quantization for large language models. In *International Conference on Machine Learning*, pp. 38087–38099. PMLR, 2023a.
- Xiao, G., Tian, Y., Chen, B., Han, S., and Lewis, M. Efficient streaming language models with attention sinks. arXiv preprint arXiv:2309.17453, 2023b.
- Xu, J., Liu, X., Wu, Y., Tong, Y., Li, Q., Ding, M., Tang, J., and Dong, Y. Imagereward: Learning and evaluating human preferences for text-to-image generation. *Advances in Neural Information Processing Systems*, 36, 2024.
- Yang, Z., Teng, J., Zheng, W., Ding, M., Huang, S., Xu, J., Yang, Y., Hong, W., Zhang, X., Feng, G., et al. Cogvideox: Text-to-video diffusion models with an expert transformer. arXiv preprint arXiv:2408.06072, 2024
- Yu, W., Luo, M., Zhou, P., Si, C., Zhou, Y., Wang, X., Feng, J., and Yan, S. Metaformer is actually what you need for vision. In *Proceedings of the IEEE/CVF conference on computer vision and pattern recognition*, pp. 10819–10829, 2022.
- Zhang, J., wei, J., Zhang, P., Zhu, J., and Chen, J. Sageattention: Accurate 8-bit attention for plug-and-play inference acceleration, 2024. URL https://arxiv.org/abs/2410.02367.
- Zhao, T., Fang, T., Liu, E., Rui, W., Soedarmadji, W., Li, S., Lin, Z., Dai, G., Yan, S., Yang, H., Ning, X., and Wang, Y. Vidit-q: Efficient and accurate quantization of diffusion transformers for image and video generation, 2024.
- Zheng, Z., Peng, X., Yang, T., Shen, C., Li, S., Liu, H., Zhou, Y., Li, T., and You, Y. Open-sora: Democratizing efficient video production for all, March 2024. URL https://github.com/hpcaitech/Open-Sora.